ADVANCED MATERIALS TECHNOLOGIES
www.advmattechnol.de

Development of Functional Filter Materials for Virus Protective Face Masks

Fatemeh Zabihi, Janina Reissner, Anika Friese, Maiko Schulze, Chuanxiong Nie, Philip Nickl, Leon Lehmann, Paul Siller, Christoph Melcher, Thomas Schneiders, Thomas Gries, Uwe Rösler, and Rainer Haag**

Wearing face masks during pandemics is an important protective measure against the spreading of virus-related infectious diseases. Nevertheless, the risk of indirect transmission of virus by handling masks is one of the earliest concerns. This problem can be minimized by supplementing the masks' textile structure with virus protective coatings. Therefore, in this concept, suitable techniques for manufacturing virus protective filter media should be evaluated. In this study, nonwoven polyamide 6 (PA6) filter material is functionalized with negatively charged linear polyglycerol sulfate (LPGS) as a virus binding functional group. Two coating conditions are investigated in which the direct covalent coating with LPGS has emerged as the optimum coating method, showing no damage to the PA6 nanofiber structure. The uncoated PA6 and LPGS-coated PA6 filter materials exhibited virus particle filtration efficiencies of 95% and 94% for airborne feline coronavirus, 98% and 86% for airborne equine herpesvirus 1(EHV-1), respectively. However, the SARS-CoV-2 absorption assay in solution indicates that the LPGS coating reduces viral titres up to 71% when incubating with the LPGS-coated PA6 filter media for one-hour. Thus, such an effect is not seen for uncoated PA6 materials. These findings confirm the suitability of LPGS coating as a suitable platform for suppression the spreading of viruses in different pandemics.

1. Introduction

Acute respiratory infectious diseases caused by influenza viruses, rhinoviruses, and coronaviruses have caused significant human health risks globally.[1] Coronaviruses, namely SARS-CoV, MERS-CoV, and the recent SARS-CoV-2, have been a significant concern for public health. These are transmitted via droplets, aerosols, and even contaminated surfaces, and have resulted in significant fatality.[2] During the ongoing SARS-CoV-2 pandemic, scientific evaluations have demonstrated that wearing a face mask is an effective non-pharmacologic intervention to minimize community spread of diseases. Recently, the effectiveness of face masks against viral transmission has been extensively studied in terms of source control and personal protection for both exhalation and inhalation of infectious virus. As source control, masks block the exhalation of virus-containing droplets into the air. As personal protection, they form a barrier against virus-contaminated droplets and aerosols from inhaled air.[3]

Face masks available in the market including cloth masks and those with polymeric filters offer varying levels of protection.[4] Indeed, filtration efficiency is a key safety parameter to determine the performance of the different face masks.[5] Several studies have shown that cloth masks do not provide high filtration efficiency for sub-micron or even larger aerosols and droplets.[6] Polyurethane face masks have been extensively used in filtering airbornes and especially air pollutants.[7] Currently, disposable face masks made from polymeric fabrics are highly recommended for air filtration.[8] These masks are usually produced in three layers as surgical face masks, using meltblown nonwoven filter in the middle and two spunbond fabric outer layers. Materials commonly used for meltblown and spunbond are nylon, polypropylene, and polystyrene.[9] In addition to surgical face masks, N95 and FFP2 masks are made in five layers: three inner nonwoven filters and two outer spunbond, a configuration that exhibits higher filtration efficacy.[3a,10] But significant limitations are seen: a significant increase of discomfort and decrease in breathability from surgical masks to FFP2 or N95 masks.[11]

F. Zabihi, M. Schulze, C. Nie, P. Nickl, L. Lehmann, R. Haag
Department of Chemistry and Biochemistry
Freie Universität Berlin
14195 Berlin, Germany
E-mail: haag@chemie.fu-berlin.de
J. Reissner, A. Friese, P. Siller, U. Rösler
Institute for Animal Hygiene and Environmental Health
Department of Veterinary Medicine
Freie Universität Berlin
14163 Berlin, Germany
E-mail: uwe.roesler@fu-berlin.de
C. Melcher, T. Schneiders, T. Gries
Institut für Textiltechnik und Lehrstuhl für Textilmaschinenbau
Otto-Blumenthal-Str. 1, 52074 Aachen, Germany

The ORCID identification number(s) for the author(s) of this article can be found under https://doi.org/10.1002/admt.202300141

DOI: 10.1002/admt.202300141

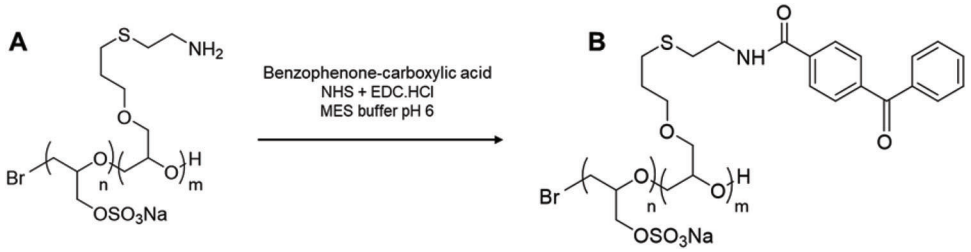

Figure 1. Schematic representation of structures of (A) LPGS-*b*-NH_2 and (B) LPGS-*b*-BPh the reaction condition.

Their comparative efficacy aside, when these masks are used, captured viruses remain active on their surface for some time, affecting the actual efficiency of the mask. In addition, disposal of the mask may also increase rather than decrease the indirect transmission of virus.[12] Furthermore, touching disposed face masks containing active viruses can increase infection through different pathways via uptake from mucous membranes from mouth, eye, etc. Therefore, using antiviral textiles may minimize the secondary transmission of infectious viruses.[13] Moreover, the ability to disinfect and reuse antiviral textiles can significantly reduce environmental pollution.[14]

Textiles with antiviral properties are interesting not only in face masks but also in other areas of medicine such as specialty clothing, health care facilities, etc.[15] Among different compounds, carbon-derived material,[16] metals and metal oxides,[17] and antiviral polymers[18] have been investigated as materials with ability to bind viruses for modification of textiles.[19] Nonetheless, many of these efforts have failed in the industrialization step due to challenges in manufacturing processes, difficulty in scale-up of the materials, and toxicity issues.[15] To date, there have been two main techniques for the functionalization of textiles:

1) Blend electrospinning: In this technique, the antiviral material is mixed with the polymer spinning solution before electrospinning. 2) Wet chemical treatment or surface graft polymerization: This is another technique in which the antiviral material is added to the surface of fabric via improving the surface adhesion and wetting characteristics to produce the fabric's antiviral function.[20]

Polymeric materials such as polypropylene (PP) and polyamide 6 (PA6) have been widely used in the fabrication of air filter materials and respirators, especially during the SARS-CoV-2 pandemic.[21] To achieve viral protective properties, the surface of these materials can be chemically modified. Considering the virus binding potency of negatively charged polysulfates,[22] their presence on the surface of PP or PA6 fibers can be considered a useful strategy to protect against infectious viruses. In this study, we have successfully synthesized LPGS with amine (LPGS-*b*-NH_2) and benzophenone (LPGS-*b*-BPh) moieties in 200 g and 100 g scales according to our previously published works.[23] In the next step, we have used two approaches for coating LPGS to the surface of nonwoven polyamide (PA6) nanofiber via both LPGS-*b*-NH_2 and LPGS-*b*-BPh, in follow-up to earlier works by our group.[23b,24] Our results confirm that direct covalent attachment of LPGS to the surface of PA6 nanofiber is an optimum approach that does not disrupt the filter media. This approach utilizes a UV-active benzophenone moiety to simultaneously graft LPGS-*b*-BPh onto the surface of PA6 nanofiber. The use of benzophenone as a grafting group is well-suited for modifying fabric substrates, which are typically made from inert polyolefins such as PP or PA6, as their ability to abstract hydrogen atoms from a donor is activated by UV light,[25] avoiding excessive damage to the filtration media. The successful coating of the LPGS-*b*-BPh on the surface of PA6 nanofiber was characterized using contact angle, scanning electron microscope (SEM), X-ray photoelectron spectroscopy (XPS) and positively charged dye (methylene blue) absorption assays. Furthermore, the particle filtration efficiency (FE) of the uncoated PA6 and LPGS-coated PA6 filter materials was measured, 95% and 94% for feline coronavirus (FCoV), 98% and 86% for equine herpesvirus 1 (EHV-1), respectively. Moreover, SARS-CoV-2 absorption assay in solution shows the highest virus-removal for LPGS-coated PA6 as compared with uncoated PA6 filter materials. Our findings suggest that the use of LPGS-coated PA6 filter materials in the structure of face masks might help in blocking viral transmission, reinforcing the importance of face masks as a preventive measure against respiratory infectious diseases.

2. Results and Discussion

2.1. Synthesis of Polymers

Linear polyglycerol with an amine functional group (LPGS-*b*-NH_2) (**Figure 1**A) was synthesized in 200 g scale in the glass reactor according to methods published earlier by our group.[24,26] Subsequently, the synthesized polymer was purified by tangential flow filtration (TFF) method with 5 kDa membrane cutoff size. Characterization of LPGS-*b*-NH_2 by ^1H and ^{13}C nuclear magnetic resonance (NMR) spectroscopy (Figures S1–S3, Supporting Information) showed that the ratio between the signals originating from the LPGS-block and covalently linked cysteamine block was as expected for a block copolymer with 155 glycerol and 5 –NH_2 units. Gel permeation chromatography (GPC), using water as mobile phase, (Figure S4, Supporting Information) showed 20 KDa molecular weight for LPGS-*b*-NH_2. Elemental analysis showed the expected C–, H–, N–, and S– elemental-content and the presence of 87% terminal sulfate groups in the structure of LPGS-*b*-NH_2. Additionally, LPGS-*b*-BPh (Figure 1B) was synthesized according to work previously published by our group.[27] Briefly, benzophenone-carboxylic acid reacted with LPGS-*b*-NH_2 in the presence of N-hydroxysuccinimide (NHS) and 1-ethyl-3-(3-dimethylaminopropyl) carbodiimid-hydrochlorid (EDC-HCl). The reaction was stirred for 24 h under light exclusion. Details

are given in the experimental section. Characterization of LPGS-*b*-BPh by ^{1}H nuclear magnetic resonance (NMR) spectroscopy (Figure S5, Supporting Information) showed that benzophenone groups successfully attached to the LPGS-block.

2.2. Fabrication of Nonwoven PA6 Filter Material

For production of the PA6 filter material, a spunbond material was covered with PA6 nanofibers in an electrospinning process. For stable PA6 nanofiber production an electrospinning process with a 24 wt. % PA6 spinning solution (in formic acid) was investigated to define suitable process parameters. (Details can be seen in the experimental section.) Fiber morphology was investigated using SEM images (Figure S6A–F, Supporting Information).

The voltage difference between emitter and collector was varied between 40 and 55 kV in steps of 5 kV, and the diameters of the resulting PA6 nonwoven fibers were measured. They ranged from 489 ± 66 nm at 40 kV voltage difference to 292 ± 41 nm at 55 kV voltage difference (Figure S6G, Supporting Information). To quantify the influence of the spinning time on the thickness, the spinning time was varied from 5 to 15 min in steps of 5 min. This resulted in a layer thickness ranging from 3 ± 2 µm (for 5 min spinning time) to 7 ± 2 µm (for 15 min) (Figure S6H, Supporting Information). Porosimeter measurements showed that the mean pore size of the uncoated spunbond material (120.4 ± 42.2 µm) was reduced by the applied nanofibrous layers. The two-layered nonwoven showed a mean pore size of 2.5 ± 0.6 µm (after 31.25 min coating time) and 1.2 ± 0.3 µm (after 62.5 min). Furthermore, the mean flow pore size increased from 5.7 ± 0.5 mbar to 14.6 ± 1.1 mbar and 303.6 ± 19.1 mbar, respectively (Figure S6I–J, Supporting Information). The described results show that the electrospinning process can be used to produce PA6 nanofibers, to coat a PP spunbond and produce a two-layered filter structure. Depending on the chosen process parameters it is possible to control the fiber diameter as well as the layer thickness of the PA6 nanofibers, leading to a reduced porosity compared to the plain PP spunbond. This reduced porosity could be beneficial for filtration of small particles, such as microorganisms. However, there are challenges in the manufacturing process to produce homogeneous and more stable coating of PA6 on the surface of PP spunbond that should be considered in future research.

2.3. Functionalization of Nonwoven PA6 Nanofiber with LPGS

There are two big hurdles to achieving virus protective function of the filtration media by wet chemical treatment: 1) the inert nature of polyolefins, which do not have active groups for post-modification with functional molecules; 2) generating covalent coating of antiviral molecules on the surface of fibers without disturbing the fabric structure, which may impact filtration efficiency and air permeability of the fabric.[12,18b] Therefore, we investigated two coating methods for functionalization of LPGS to the surface of nonwoven PA6 nanofiber (**Figure 2**A,B).

In the first approach, we applied mussel-inspired dopamine chemistry to form an adherent layer on the surface of fibers. Dopamine with functional catechol and amino groups can be self- polymerize to form a thin layer of polydopamine on a wide range of substrates.[28] In this method, nonwoven PA6 nanofibers were immersed in aqueous solution of dopamine for 6 hours. Then, polydopamine-coated PA6 nanofibers (PDA-coated PA6) were washed with distilled water and dried in the oven at 60 °C. In the next step, PDA-coated PA6 nanofibers were immersed in an aqueous solution of LPGS-*b*-NH_2 at 80 °C for 16 h. Then treated samples (PDA-LPGS-coated PA6) were washed with distilled water and dried in the oven as before. In the second approach, to explore a simpler method that can be applied on a large scale, we covalently functionalized LPGS-*b*-BPh to the fiber surfaces by immersing nonwoven PA6 nanofibers in aqueous solutions of guanidinium chloride and LPGS-*b*-BPh. Then both sides of the materials were exposed to 366 nm UV light irradiation to initiate benzophenone cross-linking. Here, the ability of benzophenone to abstract hydrogen atoms from aliphatic C−H groups and form C−C bonds under UV irradiation resulted in the simultaneous polymerization and grafting of LPGS onto the polyamide surface. Coated filter materials were then washed with PBS buffer (PH 7.4) and distilled water, respectively, to remove excess material that had not attached to the surface of PA6 nanofibers.

2.3.1. Contact Angle and SEM Observations

It was observed by contact angle that uncoated PA6 nanofibers are hydrophobic and did not absorb water droplet. But these materials became hydrophilic after LPGS coating with both methods (Figure 2C–E). The effect of LPGS coating on nonwoven PA6 nanofibers was visualized by scanning electron microscopy (SEM) images. SEM images of the uncoated PA6 nanofibers are shown in Figure 2F,I. The SEM images of PDA-LPGS-coated PA6 nanofibers show significant changes in the morphology of the nanofibers, and micrometer-sized aggregates can be observed on the surface of the fibers (Figure 2G,J). This may affect the performance of the filter media and decrease its efficiency due to damage in the overall filter network. However, the SEM images of the nonwoven LPGS-coated PA6 nanofibers do not show any sign of morphological change after the coating process (**Figure 3**H,K). In fact, no significant difference in filtration efficiency is expected for LPGS-coated PA6 nanofibers. Therefore, the second approach to generating LPGS-coated PA6 nanofibers proved more interesting in this study's further experiments, due to its fast and straightforward processing method.

2.3.2. Characterization of Functionalized PA6 Nanofibers by X-ray Photoelectron Spectroscopy

Uncoated PA6 and LPGS-coated PA6 sample were further characterized by X-ray photoelectron spectroscopy (XPS). Newly appeared signals of C–O, C=O and sulfate, which are related to the LPGS structure, confirmed the successful attachment of LPGS on the surface of the nonwoven PA6 nanofibers; in the case of uncoated samples, such signals cannot be detected (Figure S7, Supporting Information).

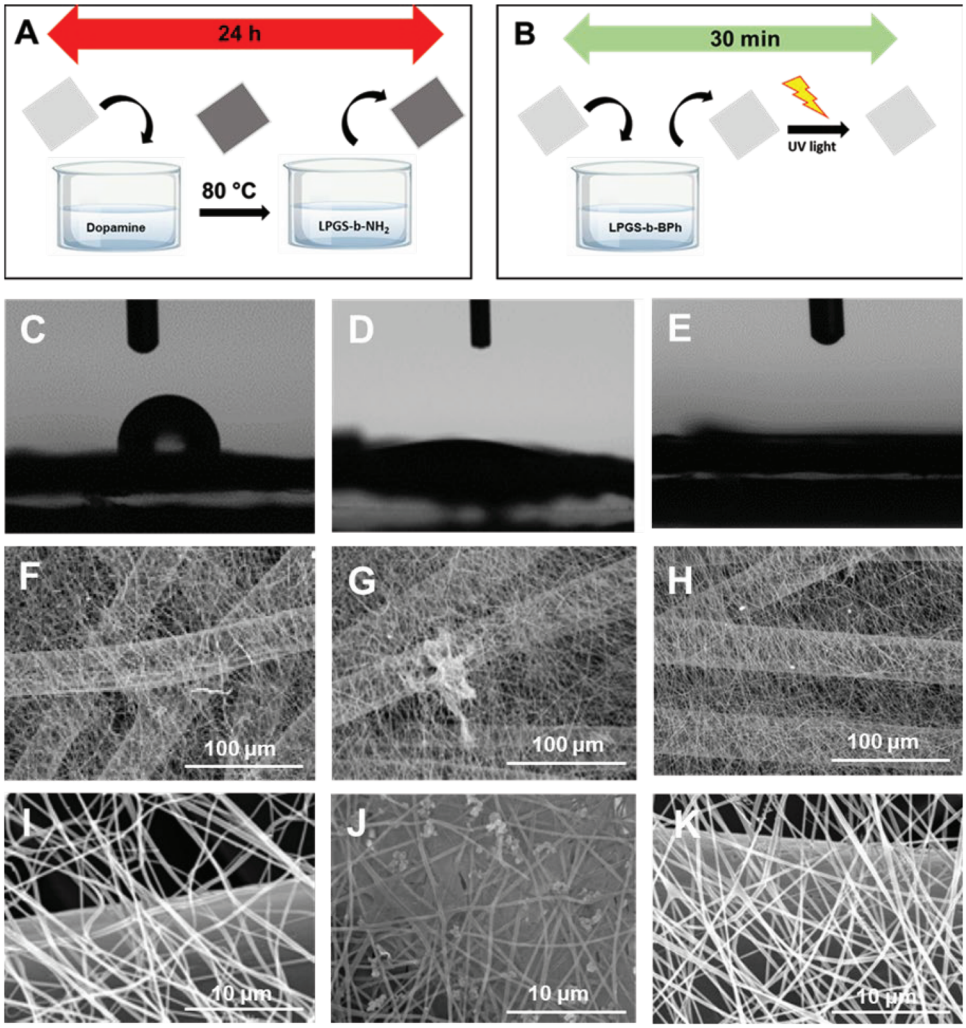

Figure 2. Schematic representation of the coating methods. A) Dopamine coating requiring two steps. First, the material is incubated in the dopamine solution for the adhesion layer, then washed and dried. Subsequently, the samples are incubated with LPGS-*b*-NH_2. B) The coating procedure for LPGS-*b*-BPh takes 30 min, in which the samples are incubated in LPGS-*b*-BPh solution with guanidinium chloride, followed by UV irradiation. C) Contact angle picture of uncoated PA6 sample shows water droplet repulsion resulting from its hydrophobic property. D,E) Contact angle pictures for PDA-LPGS- and LPGS-coated PA6 samples, respectively. The coated samples become hydrophilic and soak up water droplets. SEM images with different magnifications F,I) of nonwoven PA6 sample and G,J) PDA-LPGS-coated PA6. The adhesion layer is visible as micrometre-sized aggregates. H,K) LPGS-coated PA6; the thin coating of LPGS is not visible in the SEM images.

2.3.3. Dye Absorption Assay

LPGS-coated PA6 samples are expected to have a high negative surface charge, which is more anionic compared to uncoated samples. To confirm this property, uncoated PA6 and LPGS-coated PA6 nanofibers were incubated for 30 min in an aqueous solution of methylene blue dye (Figure 3A,B), then washed with distilled water (Figure 3C). Figure 3C demonstrates that the LPGS-coated PA6 sample shows a distinct blue color compared to the uncoated PA6 sample in the same condition. This is confirmed by electrostatic interactions between the cationic methylene blue dye and the anionic sulfate groups of LPGS-coated PA6 nanofibers, which suggests the presence of the LPGS coating on the surface of the PA6 nanofibers after treatment. Figure 3D shows a schematic representation of electrostatic interactions between methylene blue dye and the sulfate groups of LPGS. The concentration of methylene blue dye before and after incubation with uncoated PA6 and LPGS-coated PA6 samples was measured by UV–Vis spectroscopy. The difference was used to determine the amount of the dye that has been absorbed to the PA6 nanofibers surface (Figure 3E). Furthermore, the obtained values were normalized to the mass of the respective samples.

The chemical stability of the coating has been further evaluated by the dye absorption method. The uncoated PA6 and LPGS-coated PA6 samples were immersed in distilled water for 10 min and dried at room temperature (Figure S8A, Supporting Information). This step was repeated for six times and treated samples were further incubated in methylene blue dye solution for 30 min (Figure S8B, Supporting Information) and then washed with distilled water (Figure S8C, Supporting Information). The amount of the dye that has been absorbed was measured by UV spectroscopy with above mentioned method.

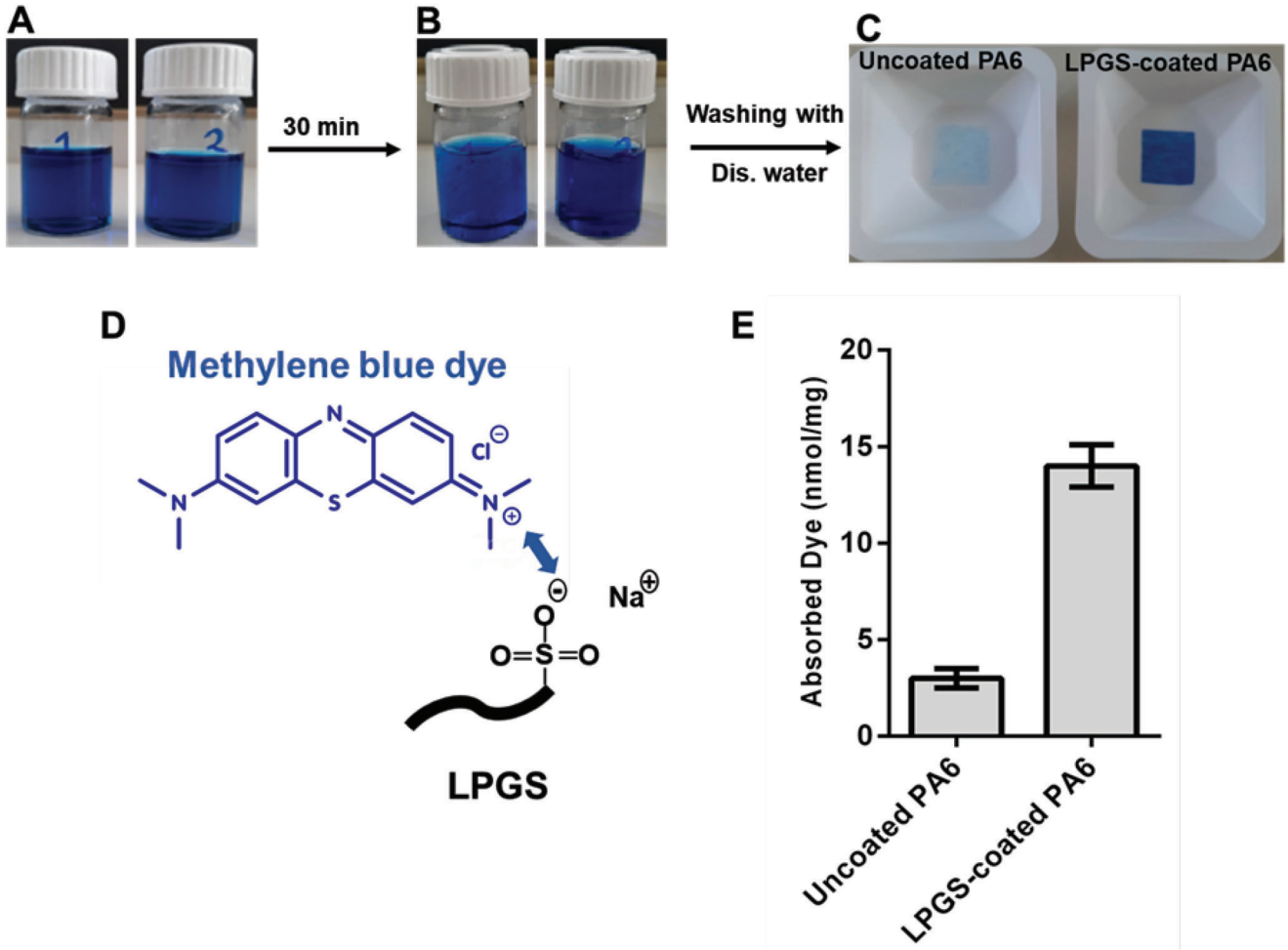

Figure 3. Absorption of methylene blue dye by uncoated PA6 and LPGS-coated PA6 nanofibers. A) Stuck solution of methylene blue 0.1 M). B) The samples are incubated on the dye solution for 30 min. C) The color of samples turn blue, but for LPGS-coated PA6 the blue color is distinct, and washing of these samples with distilled water do not remove the dye from the samples' surfaces. D) Schematic representation of the electrostatic interactions. E) Quantitative analysis of dye absorbed by samples.

Figure S8D (Supporting Information) shows absorption of dye was not changed after repeated washing step. This is further confirmed by covalently and stable coating of LPGS.

2.4. Filtration Efficiency Assay with Bioaerosols

To characterize the physical viral filtration efficiency (FE) of uncoated PA6, LPGS-coated PA6 and PDA-LPGS-coated PA6 nanofibers against airborne FCoV and EHV-1, we used an experimental setup that was previously applied successfully.[5b] The data regarding FCoV are shown in **Figure 4**A. We investigated the uncoated PA6 and the LPGS-coated PA6 filter materials in both single layer (SL) and double layer (DL). Commercial face masks, such as surgical or FFP2 masks are constructed with at least two layers.[10] Therefore, in addition to SL filter materials, we sought to investigate the effects on viral FE when using the PA6 filter materials in DL. The uncoated PA6 filter materials used in SL showed a mean viral FE of 95% (range: 87–99%) against airborne FCoV. In DL we observed a mean viral FE of 92% (range: 84–97%) for the uncoated PA6 materials. The LPGS-coated PA6 materials achieved a mean viral FE of 94% (range: 89–96%) when used in SL. As DL its mean viral FE was 88% (range: 70–99%).

In DL the LPGS-coated fabric showed a higher variation in comparison to the LPGS-coated SL. This is not recommended. Therefore, we only tested if there was a significant difference between the LPGS-coated PA6 in SL and the uncoated PA6 in SL. We defined an acceptable equivalence margin (M) to 4% which means the 95% confidence interval (CI) has to lie within the interval −4 to +4. As a result, there was no significant difference between the uncoated and LPGS-coated PA6 samples when used in SL (*CI [-1.95,3.55]*), indicating that the coating process does not disrupt the PA6 nanofiber structure in this experiment– a result confirmed by the SEM images. Since the viral FE of the nonwoven PA6 materials were not increased by using them in DL, they could be used in SL to enhance breathability. The PDA-LPGS-coated sample was only tested in SL. As you can see from the boxplot in Figure 4A, the PDA-LPGS-coated fabric had a significantly lower viral FE of 26% (range: 0–47%) in comparison to all other textiles. Therefore, it is not relevant in practice and does

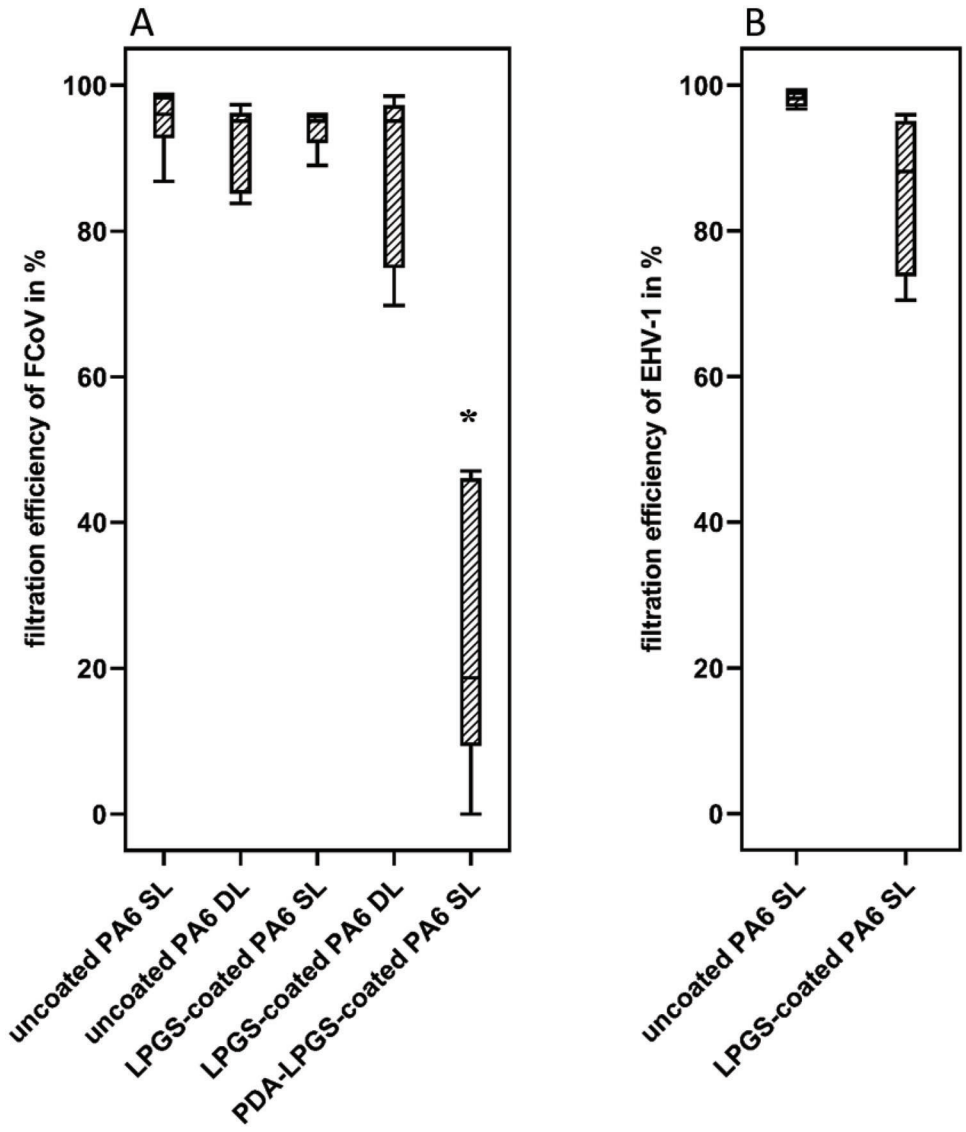

Figure 4. Viral filtration efficiency of different tested uncoated and coated PA6 nanofibers against airborne FCoV A) and airborne EHV-1 B). Experiments with FCoV were repeated five times each, with EHV-1 four times. The bold lines indicate the median and the whiskers indicate min to max values. SL = single layer, DL = double layer.

not require further statistical testing. The ultrathin LPGS coating did not change physical entrapment of viral particles. As we have already seen macroscopically changes confirmed by the SEM images, the PDA-LPGS-coated PA6 nanofibers structures seem to have been damaged by the coating process due to the long exposure time to various solutions used in the coating. This resulted in a significant loss of viral FE compared to the uncoated PA6 samples (69%,). Figure 4B presents the data on viral FE against EHV-1. Here, we investigated the filter materials in SL only after consideration of the results on FCoV. PDA-LPGS-coated samples were excluded due to their unsatisfactory results for FCoV. For the uncoated PA6 samples, we observed a mean viral FE of 98% (range: 97–99%) against EHV-1. The LPGS-coated samples achieved a lower viral FE of 86% (range: 70–96%;). The variations we saw between the individual samples of one group may result from challenges in the electrospinning manufacturing process for the PA6 nanofibers. Therefore, this challenge further in combination with LPGS coating process should be more standardized in the future works.

Possible inconsistencies in the diameter of the nanofibers or nanobeads could cause slight differences in texture and thus, in the viral FE of the fabrics.[29] In general, face masks are subjected to a series of tests. With regards to their filtration efficiency, a distinction is made between particulate filtration and bioaerosol filtration (viral FE). The NaCl method, measuring particles in a size range of 10 nm to 10 µm, is a standard testing method for evaluating the particulate FE of respirators. Using this test method the particulate FE of FFP2 masks should be at least 95%.[30] Due to very high humidity in our test chamber, particle counting with a laser-based particle counter was not possible, so we only examined the viral FE. However, the ultrasonic nebulizer used here generates particles with an initial size of 13 µm. Previous

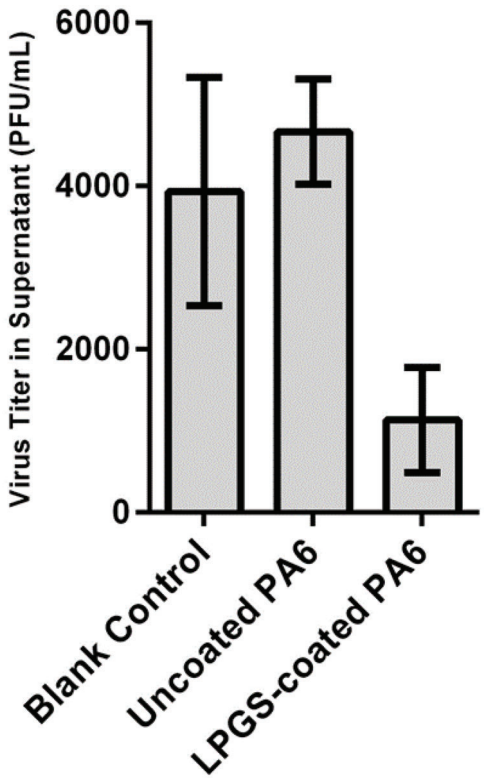

Figure 5. Removal of SARS-CoV-2 after one-hour incubation with uncoated PA6 and LPGS-coated PA6 nanofiber materials. Samples were incubated with SARS-CoV-2 suspension and the virus titres were measured using plaque assay. The experiment was repeated three times.

particle measurements at 30% relative humidity have shown that 80.5% of all particles were in a respirable size range, namely <5 μm.[5b] Although the NaCl method does not measure viral FE, this 95% could be an acceptable reference value, as viruses in aerosols are always bound to particles of different size ranges.[5b,31] N95 and FFP2 masks provide high particulate FE for crystalline particles while showing low breathability over time.[32] Therefore, high FE – especially for airborne virus particles – and sufficient air permeability are particular challenges for air filter materials. The tested materials represent an alternative approach. They achieved similarly high viral FEs, and since they were just as effective in SL, they may also offer better breathability. However, as with any type of mask, the exact fit of the mask influences its real-world efficiency.[33] Indeed, in our experimental setup, we used flat samples, which can be considered to have an ideal fitting.

2.5. Removal of SARS-CoV-2 in Suspension

We then tested if the uncoated PA6 and LPGS-coated PA6 nanofibers could remove SARS-CoV-2 in suspension. Herein, samples were incubated with SARS-CoV-2 suspensions for 1 h (SARS-CoV2M; BetaCoV/Germany/BavPat1/2020) and then virus in the supernatant was titrated by plaque assays.[22a,34] The results are shown in **Figure 5**. Clearly, the LPGS-coated PA6 nanofibers showed strong binding and absorption toward SARS-CoV-2 after one-hour of contact, with up to 71% viral removal compared with blank control. The mechanism of action could be the electrostatic interaction of negatively charged sulfate groups of LPGS with the positively charged moiety of viral spike protein, leading to virus binding and removing virus from solution; the same effect has been shown by methylene blue dye.[22a,35] We also noticed that the uncoated PA6 nanofibers did not bind to viruses in the solution due to nonspecific interactions and no binding sites between SARS-CoV-2 and uncoated PA6 nanofibers. Therefore, modifying mask filter materials increase specific interactions of viruses within contact surfaces and reduces the transmission of infectious viruses.

3. Conclusion

To create virus protective coating on the surface of nonwoven PA6 nanofibers, negatively charged linear polyglycerol sulfates (LPGS) with amine and benzophenone moieties LPGS-*b*-NH_2 and LPGS-*b*-BPh were synthesized in 200 and 100 g scale, respectively. The successful coating was characterized by contact angle, XPS, SEM and dye absorption assay. The uncoated PA6 and LPGS-coated PA6 materials were tested for viral filtration efficiency against airborne FCoV and EHV-1 viruses. As it is expected from the SEM images, the ultrathin layer of LPGS-*b*-BPh coating did not significantly changes the physical entrapment of virus particles in filtration efficiency test in comparison to uncoated material. Then, the virus removal assay was performed for uncoated PA6 and LPGS-coated PA6 filter materials, against SARS-CoV-2 suspension. We showed that the treated nanofibers displayed efficient virus removal behavior against SARS-CoV-2 after 1 h of incubation, with up to 71% viral removal, while such a strong effect was not shown for uncoated PA6 filter materials. The results show that this coating is a promising approach to treat nanofibers to improve the antiviral effect of masks and other textiles in the future.

4. Experimental Section

Materials: All chemicals and solvents obtained from Sigma–Aldrich (St. Louis, MO, USA) without further purification unless it was stated. Allyl glycidyl ether (AGE) stored over molecular sieves and before use was purified by stirring over CaH2, distillation in vacuum. Ethoxyethyl glycidyl ether (EEGE) was synthesized from 2,3-epoxypropan-1-ol (glycidol) and ethyl vinyl ether according to the literature.[36] Dopamine hydrochloride, MOPS, 2-morpholin-4-ylethanesulfonic acid (MES buffer) and PBS buffers, were obtained from Sigma–Aldrich (St. Louis, MO, USA).

Synthesis of LPGS-b-NH2: LPGS-*b*-NH_2 was synthesized according to our previously published works[24,26–27] in 200 g scale using the glass reactor. Briefly, a linear block copolymer of acetal-protected glycidol (EEGE) (192 mL, 1.234 mol) and allyl glycidyl ether (AGE) (17 mL, 0.144 mol) was synthesized via anionic ring-opening polymerization. After acetal deprotection under acidic condition and subsequently sulfating the synthesized polymer (LPGS), to obtain the amine groups on the structure of LPGS, the allyl groups were coupled with cysteamine via thiolene reaction. Descriptions of the synthetic procedures are given in the Supporting Information.

Synthesis of LPGS-b-BPh: LPGS-*b*-NH_2 block copolymer (70 g, contains 12.5 mmol of amines) was dissolved in 500 mL 2-morpholin-4-ylethanesulfonic acid (MES buffer, pH 4.8). Benzophenone-carboxylic acid (100 mmol, 8 equivalents) was dissolved in 500 mL methanol and added to the reaction. The pH of the solution adjusted to six by adding dropwise NaOH (1M). Then, N-Hydroxysuccinimide (NHS) (90 mmol, 7 equiva-

lents) and 1-Ethyl-3-(3-dimethylaminopropyl) carbodiimid-hydrochlorid (EDC-HCl), (180 mmol, 15 equivalents). The reaction was stirred under light exclusion for 24 h. Purification was done first in water/methanol mixture (4:1) in TFF with flow rate of 100 mL min^{-1} also under light exclusion for 48 h. The last step water/methanol mixture (4:1) changed to water for more 8 h (Figure S9, Supporting Information).

Fabrication of Nonwoven PA6 Filter Material: In the following experiments polypropylene (PP) spunbond nonwovens (Hagulan, Schneider Technologies GmbH + Co. KG) were used as a substrate. They were coated by electrospinning PA6 fibers onto the surface of the substrate to create a two-layer structure. The PA6 (Sigma–Aldrich (St. Louis, MO, USA) fibers (24 wt.% in formic acid (CH_2O_2, Carl Roth GmbH & Co. KG)) were produced in an electrospinning process at 30 °C, 30 % relative humidity, a nozzle-collector-distance of 20 cm and a flow rate of 0.25 ml h^{-1}. The total voltage between the emitting nozzle and the collector varied between 40 – 55 kV. All experiments were performed using a Fluidnatek LE-500 (Bioinicia SL., Valencia, Spain). To determine the layer thickness, aluminum foil was fixed on a cylindrical collector (ø = 3.2 cm) and coated with PA6 nanofibers for 5, 10, and 15 min at the same process parameters as described above. The layer thickness was then measured using a thickness gauge (F1101-30, Käfer Messuhrenfabrik, GmbH & Co. KG, Villingen-Schwenningen, Germany). For the coating process, the spunbond material was fixed on a cylindrical collector (ø = 20 cm) and rotated at 100 rpm. By applying a voltage difference between the nozzle and the collector, PA6 nanofibers were deposited on the spunbond surface. To achieve comparable layer thicknesses as generated using the 3.2 cm collector, the coating time was calculated to 31.25 and 62.5 min. The morphology of the fibers was then analyzed using SEM imaging. To measure the mean pore size of the samples, a porosimeter (PSM 165, Topas GmbH, Dresden, Germany) was used.

Coating Procedures—Coating Procedure with LPGS-b-NH_2: PA6 samples with dimension of 17,8 cm x 16 cm was placed in a fresh solution of dopamine hydrochloride (30 mL, 2 mg mL^{-1}) in MOPS buffer (0.1M, pH 7.5) and were incubated under constant shaking for 6 h. The fibers were then washed thoroughly with distilled water and dried at 60 °C for 3 h. Dopamine coated PA6 samples were placed in a solution of LPGS-*b*-NH2 (20 mL, 1 mg mL^{-1}) in MOPS buffer (0.1M, pH 8.5). The mixture was heated to 80 °C for 16 h. Subsequently, the fibers were washed thoroughly with water and dried at 60 °C.

Coating Procedure with LPGS-b-BPh: For surface modification of PA6 fibers by LPGS-*b*-BPh, PA6 fibers were cut into pieces of 17,8 cm x 16 cm. The samples were soaked in ethanol and distilled water respectively for 5 min. Immediately, they were incubated in an aqueous solution of guanidinium chloride (25 mL, 1M) for 5 min. Afterward, aqueous solution of LPGS-*b*-BPh (2 mL, 2 mg mL^{-1}) was added on the surface of fibers and incubated further 5 min. The treated PA6 samples with LPGS-*b*-BPh were irradiated with UV light for 5 min on each side in dark. The samples were washed thoroughly with PBS buffer 7.4 and with water and then dried at 60 °C for 16 h.

Experimental Setup for the Aerosol Experiments: The filtration efficiency of non-woven PA6, LPGS-coated PA6 and PDA-LPGS-coated filter materials was tested against aerosolized FCoV and EHV-1. In a previous work by Siller and colleagues, a miniaturized aerosol chamber with a volume of 80 liters was described, in which the aerosol experiments were carried out.[5b] In brief, the aerosol chamber was divided into two equal compartments by a wall with a cutout of 50 cm^2. The fabric was fixed in this cutout. The viral aerosol was generated by an ultrasonic nebulizer (Sono-Tek, Milton, NY, USA) and directed into the first compartment of the chamber. It was then passed through the fabric from the first to the second compartment by a pressure gradient generated by an all-glass impinger 30 (AGI-30, Neubert Glas GbR, Geschwenda, Germany, VDI Norm 4252–3) at a flow rate of 12.5 l min^{-1}. After a flooding time of 7 min, air samples were taken for 15 min from both compartments in parallel using two AGI-30 at a flow rate of 12.5 l min^{-1}. Therefore, all AGI-30 were connected to vacuum pumps (Leybold S4B, Leybold, Cologne, Germany and Edwards RV3, Edwards, Feldkirchen, Germany) for generating the appropriate air flow. They were filled with 30 ml of Dulbecco's Modified Eagle Medium (DMEM High Glucose, Biowest, Nuaillé, France) supplemented with 1% fetal bovine serum (FBS, PAN Biotech, Aidenbach, Germany), 1% of a mixture of 10,000 IU mL^{-1} Penicillin and 10,000 µg mL^{-1} Streptomycin (P/S, Biochrom AG, Berlin, Germany) and 50 µl autoclaved linseed oil. After sampling, the air samples were filtered with 0.22 µm filters (Roth, Karlsruhe, Germany) and stored at −80 °C until titration. To determine the viral FE of the fabrics, the concentrations of infectious viruses per m^3 of air from the air samples of the first and second compartment were calculated using an endpoint dilution assay and the ratio between the concentrations was determined. In the trials with FCoV, the uncoated PA6 and LPGS-coated PA6 fabrics were tested five times each in single layer (SL) and double layer (DL). In the trials with EHV-1, they were tested four times in SL. The PDA-LPGS-coated fabric was only tested for FCoV and only in SL five times.

Preparation of Virus Stocks: The FCoV strain that it used as a surrogate for SARS-CoV-2 was provided by the Friedrich Loeffler Institute (FLI, Isle of Riems, Germany; viral registration number RVB-1259). It was grown in Crandell-Rees Feline Kidney (CRFK) cells (ATTC CCL-94). Furthermore, it used EHV-1 as a surrogate for herpes simplex virus. EHV-1 was grown in Rabbit Kidney (RK-13) cells. They were kindly provided by the Institute of Virology, department of veterinary medicine, Freie Universitaet Berlin. The virus stocks were propagated according to our previously published work.[5b] DMEM supplemented with 10% FBS and 1% P/S was used as cell culture media. For the quantification of the virus titers, it used endpoint dilution assays. They were performed in 96-well plates with confluent host cells. After an incubating time of three to five days at 37 °C and a 5% CO_2 atmosphere it looked for cythopathic effects (CPE). Viral titers were then calculated according to the Spearman-Karber method[37] and expressed as tissue culture infectious dose 50 ($TCID_{50}$). For the aerosol experiments, the initial FCoV concentration was adjusted to approximately $10^{6.225}$ and the EHV-1 concentration to $10^{6.7}$ $TCID_{50}$/mL.

Statistical Analysis: The data were analyzed using an equivalence trial. As you can see from the boxplot in Figure 4, the PDA-LPGS-coated fabric had a significantly lower FE and did not require testing. In DL the fabrics showed a higher variation, which results in a lower reliability of the equivalence trial. Therefore, it only tested if there was a significant difference between the LPGS-coated PA6 in SL and the uncoated PA6 in SL. The acceptable equivalence margin (M) was set to 4%. They were considered equivalent if the 95% confidence interval (CI) lies within the interval −4 to +4. Graphpad Prism 8 (GraphPad Software, San Diego, CA, USA) was used for creating Figure 4.

Virus Removal Experiment of SARS-CoV-2: SARS-CoV-2 München (SARS-CoV2M; BetaCoV/Germany/BavPat1/2020) was propagated on Vero E6 cells and quantified by plaque assay according to literature.[22a] The samples were immersed in SARS-CoV-2 suspensions for 1 h at r.t. and then the virus in the suspension was titrated on Vero E6 cells. The experiments were performed in a BSL3 laboratory at the Institut für Virology, Freie Universität Berlin.

Instruments—Scanning Electron Microscopy (SEM): Nonwoven PA6 samples with and without LPGS functionalization were sputtered with gold to obtain a conductive layer of at least 5 nm thickness, using a compact coating unit CCU-010 by Safematic GmbH (Bad Ragaz, Switzerland). Images were obtained using an SU8030 field-emission scanning electron microscope (FE-SEM) by Hitachi (Tokyo, Japan). The accelerating voltage (*Vac*) was set to 20 kV, the current to 20 µA, and the working distance was 21.6 cm.; Contact Angle: Contact angle measurements were performed using the contact angle goniometer OCA20 (Dataphysics Instruments, Filderstadt, Germany). A droplet of water (2 µL) was gently placed on the respective surface of the fibers and allowed to equilibrate for 10 s. The shape of the droplet was recorded and evaluated using the software SCA20 (Dataphysics Instruments, Filderstadt, Germany). Contact angle values were not determined due to the uneven texture surfaces of PA6 nonwoven fibers. X-ray photoelectron spectroscopy (XPS): XP spectra were recorded on a Kratos (Manchester, UK) Axis Ultra DLD spectrometer, equipped with a monochromatic Al Kα X-ray source. The spectra were measured in normal emission, and a source-to-sample angle of 60° was used. All spectras were recorded utilizing the fixed analyzer transmission (FAT) mode. The binding energy scale of the instrument was calibrated, following a technical procedure provided by Kratos Analytical Ltd (calibration was performed according to ISO 15472) The spectra were recorded

utilizing the instrument's slot and hybrid lens modes. An analysis area of ≈300 µm x 700 µm was investigated; charge neutralization was applied. For quantification, the survey spectra were measured with a pass energy of 80 electron volt (eV), and the spectra were quantified utilizing the empirical sensitivity factors that were provided by KRATOS (the sensitivity factors were corrected with the transmission function of the spectrometer). The high-resolution XPS spectra were measured with a pass energy of 20 eV, and the respective data were processed using UNIFIT 2019 spectrum processing software. For fitting, a Shirley background and a Gaussian/Lorentzian sum function (peak shape model GL (30)) were used. If not denoted otherwise, the L-G mixing component was set to 0.35 for all peaks. In case of the C1s spectra, peak fitting was performed in such a manner that all residual structures were removed, and all binding energies were calibrated to the signal observed for the aliphatic C–C bond component (observed at 284.8 eV).; Ultraviolet (UV): UV light irradiation during the coating procedure was done at 366 nm using a Camag laboratory UV lamp (Muttenz, Switzerland) at a constant distance with a power of 2.3 µW cm^{-2}. Gel permeation chromatography (GPC): GPC measurement was performed in water using an Agilent 1100 (Agilent Technologies). The instrument equipped inside with a degasser, a pump, a UV detector and a RI detector. For sample separation, 50 µL of solution with a concentration of 6 mg mL^{-1}, was injected through a precolumn and three columns with a particle size of 10 µm were used at room temperature. The calibration standard was Pullulan and the solvent water with 0.1 M NaNO3. Tangential flow filtration (TFF): Purification of the synthesized materials were performrd using TFF method in water or water/methanol mixture, which it is equipped with Quattroflow 150S Quaternary pump (PSG Germany GmbH). The pump is a four-piston diaphragm pump. The four segments of the pump diaphragm oscillate back and forth. The sample flowed vertically through a tube onto a membrane with 2000 MWCO with flow rate of 100 mL min^{-1}, allowing small molecules to pass through the membrane and be separated and washed into waste. The purified sample was retured into the sampel flask again and was continuously purified and recycled. This movement was created by a connector to the pump. Also a constant volume of washing solution were added into the sample flask. Figure S5 (Supporting Information) shows the technical operation of the TFF purification.

Supporting Information

Supporting Information is available from the Wiley Online Library or from the author.

Acknowledgements

This work was supported by Bundesministerium für Bildung und Forschung (BMBF) with grant number 13GW0544E. The authors thank Core Facility Bio SupraMol (Freie UniversitätBerlin) for the use of their research and analytical facilities. Prof. Benedikt Kaufer, Dr. Jakob Trimpert and Julia-Maria Adler were acknowledged for performing the SARS-CoV-2 experiments. Ben Allen and Cathleen Hudziak were also thanked for language editing of the manuscript and GPC measurement, respectively.

Open access funding enabled and organized by Projekt DEAL.

Conflict of Interest

The authors declare no conflict of interest.

Data Availability Statement

The data that support the findings of this study are available in the supplementary material of this article.

Keywords

face masks, nonwoven PA6 nanofibers, virus protective coatings, LPGS-*b*-BPh, viral filtration efficiencies

Received: January 31, 2023
Revised: May 16, 2023
Published online: June 17, 2023

[1] a) J. L. Temte, S. Barlow, E. Temte, M. Goss, A. Bateman, K. Florek, A. Uzicanin, *Clin. Infect. Dis.* **2022**, *75*, S205; b) Y. M. Chong, Y. F. Chan, M. F. H. Jamaluddin, M. S. Hasan, Y. K. Pang, S. Ponnampalavanar, S. F. Syed Omar, I. C. Sam, *PLoS One* **2022**, *17*, e0273697.

[2] a) V. C. C. Cheng, J. D. Ip, A. W. H. Chu, A. R. Tam, W. M. Chan, S. M. U. Abdullah, B. P. C. Chan, S. C. Wong, M. Y. W. Kwan, G. T. Chua, P. Ip, J. M. C. Chan, B. H. S. Lam, W. K. To, V. W. M. Chuang, K. Y. Yuen, I. F. N. Hung, K. K. W. To, *Clin. Infect. Dis.* **2022**, *75*, e44; b) K. Diriba, E. Awulachew, E. Getu, *Eur J Med Res* **2020**, *25*, 39; c) S. Belluco, M. Mancin, F. Marzoli, A. Bortolami, E. Mazzetto, A. Pezzuto, M. Favretti, C. Terregino, F. Bonfante, R. Piro, *Eur J Epidemiol* **2021**, *36*, 685; d) I. D. Amoah, L. Pillay, N. Deepnarian, O. Awolusi, K. Pillay, P. Ramlal, S. Kumari, F. Bux, *International Journal of Hygiene and Environmental Health* **2021**, *236*, 113807.

[3] a) Y. Cheng, N. Ma, C. Witt, S. Rapp, P. S. Wild, M. O. Andreae, U. Pöschl, H. Su, *Science* **2021**, *372*, 1439; b) J. Howard, A. Huang, Z. Li, Z. Tufekci, V. Zdimal, H.-M. van der Westhuizen, A. von Delft, A. Price, L. Fridman, L.-H. Tang, V. Tang, G. L. Watson, C. E. Bax, R. Shaikh, F. Questier, D. Hernandez, L. F. Chu, C. M. Ramirez, A. W. Rimoin, *Proc. Natl. Acad. Sci. USA* **2021**, *118*, e2014564118.

[4] A.-M. Park, S. Khadka, F. Sato, S. Omura, M. Fujita, K. Hashiwaki, I. Tsunoda, *Sci. Rep.* **2022**, *12*, 11361.

[5] a) H. E. Whyte, Y. Montigaud, E. Audoux, P. Verhoeven, A. Prier, L. Leclerc, G. Sarry, C. Laurent, L. Le Coq, A. Joubert, J. Pourchez, *Sci. Rep.* **2022**, *12*, 1188; b) P. Siller, J. Reissner, S. Hansen, M. Kühl, A. Bartel, D. Schmelzeisen, T. Gries, U. Roesler, A. Friese, *Nanomaterials* **2021**, *11*, 2088.

[6] a) K. M. Shakya, A. Noyes, R. Kallin, R. E. Peltier, *J Expo Sci Environ Epidemiol* **2017**, *27*, 352; b) S. Rengasamy, B. Eimer, R. E. Shaffer, *Ann Occup Hyg* **2010**, *54*, 789.

[7] Z. Sun, W. Guo, C.-K. Chan, L. Jin, S. M. Griffith, J. Z. Yu, W. Chan, *Chem. Res. Toxicol.* **2022**, *35*, 1604.

[8] a) A. Davies, K. A. Thompson, K. Giri, G. Kafatos, J. Walker, A. Bennett, *Disaster Med Public Health Prep* **2013**, *7*, 413; b) M. Vincent, P. Edwards, *Cochrane Database Syst Rev* **2016**, https://doi.org/10.1002/14651858.CD002929.

[9] A. B. Dogan, K. E. Dabkowski, J. L. Cadnum, C. J. Donskey, H. A. von Recum, *Ann. Biomed. Eng.* **2022**, *51*, 833.

[10] G. Korkmaz, M. Kılınç, S. A. Razak, M. Ocak, S. Korkmaz, Y. D. T. Kut, *The Journal of The Textile Institute* **2022**, *114*, 250.

[11] S. Fikenzer, T. Uhe, D. Lavall, U. Rudolph, R. Falz, M. Busse, P. Hepp, U. Laufs, *Clin. Res. Cardiol.* **2020**, *109*, 1522.

[12] A. Cano-Vicent, A. Tuñón-Molina, M. Martí, Y. Muramoto, T. Noda, K. Takayama, Á. Serrano-Aroca, *ACS Omega* **2021**, *6*, 23495.

[13] S. Schorderet Weber, X. Bulliard, R. Bonfante, Y. Xiang, S. Biselli, S. Steiner, S. Constant, R. Pugin, A. Laurent, S. Majeed, S. Lebrun, M. Palmieri, A. Hogg, A. Kuczaj, M. C. Peitsch, J. Hoeng, A. Stan, *Sci. Rep.* **2022**, *12*, 17041.

[14] I. Armentano, M. Barbanera, E. Carota, S. Crognale, M. Marconi, S. Rossi, G. Rubino, M. Scungio, J. Taborri, G. Calabrò, *ACS Appl Polym Mater* **2021**, *3*, 531.

[15] I. Rubino, H. J. Choi, *Trends Biotechnol.* **2017**, *35*, 907.

[16] C. Mu, J. Ren, H. Chen, Y. Wu, Q. Xu, X. Sun, K. Yan, *ACS Appl. Nano Mater.* **2021**, *4*, 10634.
[17] a) Y. Li, P. Leung, L. Yao, Q. W. Song, E. Newton, *J Hosp Infect* **2006**, *62*, 58; b) P. Merkl, S. Long, G. M. McInerney, G. A. Sotiriou, *Nanomaterials* **2021**, *11*, 1312; c) C. A. M. Ferreira, S. F. C. Guerreiro, J. F. A. Valente, T. M. F. Patrício, N. Alves, A. Mateus, J. R. Dias, *Polymers* **2022**, *14*, 3329.
[18] a) S. Kumaran, E. Oh, S. Han, H. J. Choi, *Nano Lett.* **2021**, *21*, 5422; b) M. Sorci, T. D. Fink, V. Sharma, S. Singh, R. Chen, B. L. Arduini, K. Dovidenko, C. L. Heldt, E. F. Palermo, R. H. Zha, *ACS Appl. Mater. Interfaces* **2022**, *14*, 25135.
[19] P. D. Rakowska, M. Tiddia, N. Faruqui, C. Bankier, Y. Pei, A. J. Pollard, J. Zhang, I. S. Gilmore, *Communications Materials* **2021**, *2*, 53.
[20] Y. Zhang, W. Fan, Y. Sun, W. Chen, Y. Zhang, *Nanotechnol Rev* **2021**, *10*, 1092.
[21] D. Battegazzore, F. Cravero, A. Frache, *Polymers* **2020**, *12*, 2726.
[22] a) C. Nie, P. Pouyan, D. Lauster, J. Trimpert, Y. Kerkhoff, G. P. Szekeres, M. Wallert, S. Block, A. K. Sahoo, J. Dernedde, K. Pagel, B. B. Kaufer, R. R. Netz, M. Ballauff, R. Haag, *Angew. Chem., Int. Ed.* **2021**, *60*, 15870; b) V. Ahmadi, C. Nie, E. Mohammadifar, K. Achazi, S. Wedepohl, Y. Kerkhoff, S. Block, K. Osterrieder, R. Haag, *Chem. Commun.* **2021**, *57*, 11948; c) P. S. Kwon, H. Oh, S.-J. Kwon, W. Jin, F. Zhang, K. Fraser, J. J. Hong, R. J. Linhardt, J. S. Dordick, *Cell Discov.* **2020**, *6*, 50; d) *AIDS Res. Hum. Retroviruses* **2008**, *24*, 925.
[23] a) L. Yu, C. Cheng, Q. Ran, C. Schlaich, P.-L. M. Noeske, W. Li, Q. Wei, R. Haag, *ACS Appl. Mater. Interfaces* **2017**, *9*, 6624; b) M. Schulze, C. Nie, G. Hartmann, P. Nickl, M. W. Kulka, M. Ballauff, R. Haag, *J. Appl. Polym. Sci.* **2023**, *140*, e53444.
[24] M. W. Kulka, S. Smatty, F. Hehnen, T. Bierewirtz, K. Silberreis, C. Nie, Y. Kerkhoff, C. Grötzinger, S. Friedrich, L. I. Dahms, J. Dernedde, I. Grunwald, M. Schirner, U. Kertzscher, K. Affeld, R. Haag, *Adv. Mater. Interfaces* **2020**, *7*, 2000272.
[25] a) H. Kubota, Y. Ogiwara, Y. Hata, *Polymer Photochemistry* **1986**, *7*, 389; b) O. Tretinnikov, V. Pilipenko, L. Prikhodchenko, *Polymer Science Series B* **2012**, *54*, 427; c) M. H. Schneider, H. Willaime, Y. Tran, F. Rezgui, P. Tabeling, *Anal. Chem.* **2010**, *82*, 8848.
[26] M. W. Kulka, I. S. Donskyi, N. Wurzler, D. Salz, Ö. Özcan, W. E. S. Unger, R. Haag, *ACS Appl Bio Mater* **2019**, *2*, 5749.
[27] M. Schulze, S. Adigüzel, P. Nickl, A.-C. Schmitt, J. Dernedde, M. Ballauff, R. Haag, *Adv. Mater. Interfaces* **2022**, *9*, 2102005.
[28] a) A. B. Asha, Y. Chen, R. Narain, *Chem. Soc. Rev.* **2021**, *50*, 11668; b) G. Fredi, F. Simon, D. Sychev, I. Melnyk, A. Janke, C. Scheffler, C. Zimmerer, *ACS Omega* **2020**, *5*, 19639.
[29] R. Nayak, R. Padhye, *J. Text. Eng. Fash. Technol* **2017**, *2*, 486.
[30] P. Forouzandeh, K. O'Dowd, S. C. Pillai, *Safety Science* **2021**, *133*, 104995.
[31] W. W. Nazaroff, *Indoor Air* **2022**, *32*, e12970.
[32] a) T. Hamouda, H. Kafafy, H. M. Mashaly, N. M. Aly, *J Ind Text* **2022**, *51*, 1494; b) M. H. Chua, W. Cheng, S. S. Goh, J. Kong, B. Li, J. Y. C. Lim, L. Mao, S. Wang, K. Xue, L. Yang, E. Ye, K. Zhang, W. C. D. Cheong, B. H. Tan, Z. Li, B. H. Tan, X. J. Loh, *Research* **2020**, *2020*, 7286735.
[33] J. Schmitt, J. Wang, *Indoor Air* **2022**, *32*, e13127.
[34] R. Wölfel, V. M. Corman, W. Guggemos, M. Seilmaier, S. Zange, M. A. Müller, D. Niemeyer, T. C. Jones, P. Vollmar, C. Rothe, M. Hoelscher, T. Bleicker, S. Brünink, J. Schneider, R. Ehmann, K. Zwirglmaier, C. Drosten, C. Wendtner, *Nature* **2020**, *581*, 465.
[35] a) X. Xu, M. Ballauff, *J. Phys. Chem. B* **2019**, *123*, 8222; b) X. Xu, Q. Ran, P. Dey, R. Nikam, R. Haag, M. Ballauff, J. Dzubiella, *Biomacromolecules* **2018**, *19*, 409; c) P. Pouyan, C. Nie, S. Bhatia, S. Wedepohl, K. Achazi, N. Osterrieder, R. Haag, *Biomacromolecules* **2021**, *22*, 1545.
[36] M. Gosecki, M. Gadzinowski, M. Gosecka, T. Basinska, S. Slomkowski, *Polymers* **2016**, *8*, 227.
[37] C. SPEARMAN, *Br J Psychol* **1908**, *2*, 227.